metals

MDPI

Article

Adsorption Mechanism of Eco-Friendly Corrosion Inhibitors for Exceptional Corrosion Protection of Carbon Steel: Electrochemical and First-Principles DFT Evaluations

Abdelkarim Chaouiki [1,†], Maryam Chafiq [1,†], Young Gun Ko [1,*], Aisha H. Al-Moubaraki [2], Fatima Zahra Thari [3], Rachid Salghi [4], Khalid Karrouchi [5], Khalid Bougrin [3,6], Ismat H. Ali [7] and Hassane Lgaz [8,*]

1 Materials Electrochemistry Laboratory, School of Materials Science and Engineering, Yeungnam University, Gyeongsan 38541, Korea
2 Department of Chemistry, Faculty of Sciences—Alfaisaliah Campus, University of Jeddah, Jeddah 21589, Saudi Arabia
3 Equipe de Chimie des Plantes et de Synthèse Organique et Bioorganique, URAC23, Faculty of Science, B.P. 1014, Geophysics, Natural Patrimony and Green Chemistry (GEOPAC) Research Center, Mohammed V University, Rabat 10100, Morocco
4 Laboratory of Applied Chemistry and Environment, ENSA, University Ibn Zohr, P.O. Box 1136, Agadir 80000, Morocco
5 Laboratory of Analytical Chemistry and Bromatology, Faculty of Medicine and Pharmacy, Mohamed V University, Rabat 10100, Morocco
6 Department of Chemical and Biochemical Sciences-Green Process Engineering (CBS-GPE), Mohammed VI Polytechnic University (UM6P), Ben Guerir 43150, Morocco
7 Department of Chemistry, College of Science, King Khalid University, P.O. Box 9004, Abha 61413, Saudi Arabia
8 Innovative Durable Building and Infrastructure Research Center, Center for Creative Convergence Education, Hanyang University ERICA, 55 Hanyangdaehak-ro, Sangrok-gu, Ansan-si 15588, Korea
* Correspondence: younggun@ynu.ac.kr (Y.G.K.); hlgaz@hanyang.ac.kr (H.L.)
† These authors contributed equally to this work.

check for updates

Citation: Chaouiki, A.; Chafiq, M.; Ko, Y.G.; Al-Moubaraki, A.H.; Thari, F.Z.; Salghi, R.; Karrouchi, K.; Bougrin, K.; Ali, I.H.; Lgaz, H. Adsorption Mechanism of Eco-Friendly Corrosion Inhibitors for Exceptional Corrosion Protection of Carbon Steel: Electrochemical and First-Principles DFT Evaluations. *Metals* **2022**, *12*, 1598. https://doi.org/10.3390/met12101598

Academic Editor: Branimir N. Grgur

Received: 6 August 2022
Accepted: 21 September 2022
Published: 25 September 2022

Abstract: In the present work, we represent two thiazolidinediones, namely (Z)-5-(4-methoxybenzylidene) thiazolidine-2,4-dione (MeOTZD) and (Z)-5-(4-methylbenzylidene) thiazolidine-2,4-dione (MeTZD), as corrosion inhibitors for carbon steel (CS) in 1.0 M HCl solution. Techniques for gravimetric methods, electrochemical measurements, and morphological characterization were used to conduct experimental evaluations. Additionally, calculations based on the fundamental principles of Density Functional Theory (DFT) were employed to simulate inhibitor–iron interactions. Experimental results indicated that investigated inhibitors can significantly enhance the corrosion resistance of CS, reaching a performance of 95% and 87% at 5×10^{-3} mol/L of MeOTZ and MeTZD, respectively. According to gravimetric and electrochemical experiments, inhibitor molecules obstruct corrosion reactions by adhering to the CS surface, which follows the Langmuir isotherm model. On the other hand, the morphological analysis showed a well-distinguished difference between unprotected and protected CS surfaces as a result of the inhibitors' addition to HCl. Projected density of states and interaction energies obtained from first-principles DFT simulations indicate that the studied molecules form covalent bonds with iron atoms through charge transfer.

Keywords: thiazolidinediones; first-principles DFT; corrosion inhibitor; SEM; density of states; electrochemical techniques

1. Introduction

The continuous progress of the concept of environmentally friendly chemistry has helped to answer numerous challenges faced by modern companies, technologies, and industries [1]. In this regard, the development of more environmentally friendly chemicals and techniques has been a subject of great interest in corrosion protection research [2,3].

Corrosion control is acknowledged to be necessary at both the design and operational stages. Among the highest grades of corrosion research, an increasing focus has been placed on the corrosion of different grades of carbon steel (CS) in many aggressive environments [4,5]. CS plays an important role in our daily lives; it is extensively used in domestic life and in numerous technological and industrial applications due to its low cost and excellent mechanical properties. In applications where acid solutions are used to treat steel-based equipment, such as pickling, cleaning of industrial equipment, acidization of oil wells, acid descaling, and many other industrial/chemical processes, corrosion inhibitors are the first choice against acidic corrosion [6,7]. Strong corrosion prevention properties can be found in organic compounds that feature heteroatoms like oxygen, nitrogen, sulfur, etc., in their molecular structures, together with many bonds or aromatic rings [8–12]. However, designing and synthesizing novel and effective organic corrosion inhibitors are challenging tasks. More specifically, meeting effectiveness, eco-friendly, and low-cost requirements demands a substantial research effort. Recently, thiazolidinediones have emerged as promising organic compounds with several successful applications in pharmaceutical and medical fields [13–15]. Along with their wide range of biological activities, these compounds have excellent structural features that make them promising corrosion inhibitor candidates. They have highly advantageous structural characteristics because the thiazole-derived ring contains two electron-accepting carbonyl groups as well as -NH and -S- active sites. It is anticipated that such active regions will have a special affection for metal-binding orbitals. A quick literature search reinforces this conclusion, since chemical compounds with carbon chains, functional groups, and heteroatoms possess high corrosion inhibition performance. Despite these facts, limited research efforts have been devoted to the utilization of the thiazolidine family for corrosion inhibition of materials. Some researchers have shown that thiadiazoline derivatives have excellent anticorrosion benefits and could be applied as successful anti-corrosion agents. Among these, thiadiazolines synthesized by Tiwari et al. [16] and those screened by Yadav et al. [17] stand out due to their potent anticorrosive abilities.

In accordance with these ongoing efforts, we present here the corrosion inhibition properties and adsorption mechanism of two thiazolidinedione derivatives for CS in HCl solution, namely (Z)-5-(4-methoxybenzylidene) thiazolidine-2,4-dione (MeOTZD) and (Z)-5-(4-methylbenzylidene) thiazolidine-2,4-dione (MeTZD). Attention has been given to these organic compounds because of their electron-rich molecular structures, which can make them excellent corrosion inhibitors even at low doses. Furthermore, in a very recent study by our team, two thiazolidinedione derivatives, including MeTZD, were reported as excellent corrosion inhibitors for copper in 3.5 wt.% of sodium chloride [18]. Encouraged by these results on the structural and biological features of this class of compounds, the present study was carried out with the aim to strengthen the existing knowledge as well as serve as a guide for future research in this class of organic compounds. To achieve this goal, the corrosion resistance of the compounds under consideration was assessed using a variety of experimental techniques, including scanning electron microscopy (SEM), the gravimetric method, and electrochemical measurements. Additionally, the optimal geometries of inhibitor-Fe (110) complexes and the predicted densities of states of molecules both before and after adsorption were determined using first-principles DFT calculations to examine the underlying adsorption mechanism. The adopted research approach can lead to useful conclusions about the capabilities of tested compounds as acid corrosion inhibitors.

2. Experimental Procedure

2.1. Synthesis of Inhibitor Molecules

All the methodologies outlined in the literature were used to synthesize all the named molecules reported below [19]. In brief, sodium hydroxide (1.1 mmol) was added to an equimolar mixture of thiazolidine-2,4-dione (1) (0.12 g, 1 mmol), 4-methoxylbenzaldehyde (2a), or 4-methylbenzaldehyde (2b) in water/ethanol (v/v, 2:1) (10 mL) and agitated for 7 h at room temperature (Scheme 1). TLC was used to keep track of when the reaction had finished.

Using diluted hydrochloric acid, the reaction mixture was made acidic. MeOTZD and MeTZD are pure products that were obtained after the solid was filtered and recrystallized from ethanol. The supplemental material reports on their characterization.

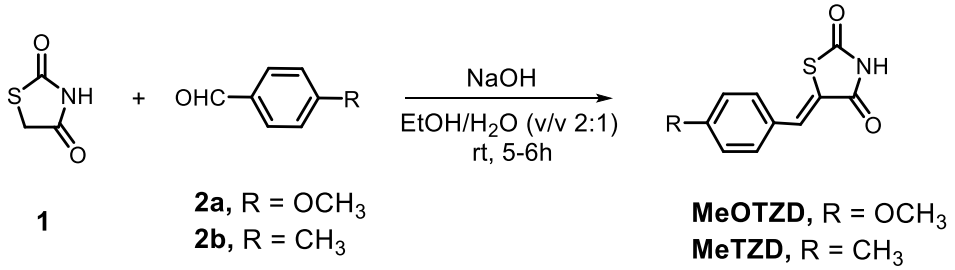

Scheme 1. General procedure for the synthesis of compounds MeOTZD and MeTZD.

2.2. Samples and Corrosive Medium

The substance under examination in this work is CS, which has the corresponding elemental make-up: 0.19 C, 0.20 Si, 0.81 Mn, 0.0027 S, 0.12 Cr, 0.001 P, 0.11 Ni, 0.18 Cu, 0.032 Al, and the rest Fe. The Sigma-Aldrich commercial acid concentrated at a 37% concentration was diluted using distilled water to establish the aggressive medium, which contains molar hydrochloric acid at a concentration of 1.0 M HCl. For electrochemical investigations, CS samples with a 1 cm^2 cross-section were employed. The samples were polished with extremely fine SiC paper (#800 to #1200) before each test, then rinsed with distilled water, degreased with acetone, and air dried. A prepared aggressive solution was tested with different inhibitor concentrations by each assay.

2.3. Gravimetric Method

Investigations evaluating weight loss (WL) were regarded as a standard approach to evaluating an inhibitor compound's capacity to stop corrosion based on ASTM protocols [20]. By submerging suitable CS specimens in corrosive medium with various concentrations of MeOTZD and MeTZD for 24 h, WL tests were carried out (303 K to 333 K). Before being submerged in the experimental solution, the rectangular-shaped coupons ($2.7 \times 2 \times 0.3$ cm^3) had their surfaces abraded using emery paper.

The following equations were used to evaluate the corrosion parameters, such as corrosion rate, inhibition performance, and surface coverage, in the presence and absence of each concentration of inhibitors [21]:

$$C_{WL} = \frac{8.76 \times \Delta W}{D \times A \times t} \tag{1}$$

$$\eta_{WL}(\%) = \left[1 - \frac{C_{WL}}{C^{\circ}_{WL}}\right] \times 100 \tag{2}$$

$$\theta = \frac{C^{\circ}_{WL} - C_{WL}}{C^{\circ}_{WL}} \tag{3}$$

where ΔW is weight loss (in milligrams), A is the area of the CS samples (in cm^2), t is exposure time in hours, D is steel specimen density in grams per cubic centimeter, C_{WL} and C°_{WL} are corrosion rates at different inhibitor concentrations and in the absence of any inhibitors, and θ is the surface coverage.

2.4. Assessment of Electrochemical Behavior Using LPR, EIS, and PDP

In order to monitor CS corrosion, electrochemical methods are increasingly used. This study made use of three electrochemical techniques: linear polarization resistance (LPR), electrochemical impedance spectroscopy (EIS), and potentiodynamic polarization (PDP). The three-electrode cell with a Volta lab potentiostat/galvanostat of the kind made by

Corrtest Instruments Corp, Ltd. was used for all electrochemical experiments (Wuhan, China). Platinum (Pt), which has a surface area of 1 cm^2, and $Hg/Hg_2Cl_2/KCl_{sat}$ (SCE), were utilized as the counter and reference electrodes, respectively. Before measurements, the working electrode, which is composed of carbon steel, was submerged with SCE in the solution for 0.5 h to achieve a constant open circuit potential (OCP) (OCP curves are shown in Figure S1, Supplementary Material). A circulating water thermostat was used to complete each measurement at 303 ± 2 K.

The measurement of EIS was done at frequencies between 100 KHz and 10 mHz, using a sinusoidal disturbance potential of 10 mV. The determination of the electrochemical impedance from the corresponding diagrams provides information on different processes concerning the corrosion inhibition ability of the inhibitors for which the protection efficiency (%) was calculated. The current-potential curves were captured for PDP measurements in the potential range of −800 to −200 mV at a scan rate of 0.5 mV s^{-1} at 303 K. Linear polarization resistance (LPR) experiments were performed from −15 to +15 mV vs. E_{corr} at the scan rate of 0.125 mV/s. The reported values of electrochemical parameters are the average values of three tests executed under similar conditions.

2.5. Computational Methods

To depict the adsorption mechanism, spin-polarized DFT simulations were employed. The structure was optimized using the CASTEP algorithm implemented in Materials Studio. Considering exchange-correlation energy, the generalized gradient approximation (GGA) with PBE parameterization was employed. An empirical dispersion correction method was used to handle the vdW interactions (DFT-D3). The plane-wave basis energy cutoff was set at 30 Ry. Convergence thresholds in the CASTEP module had preset values of "Fine" quality. The measured value (2.866) and the lattice constant determined from DFT simulations were nearly identical [22]. The Fe crystal was split into four layers in the (110) plan, which was found to be the most stable iron surface [23]. Afterward, a 5 × 5 supercell was formed. In order to take into account erroneous interactions between slabs, a 20-vacuum slab was made along the *z*-axis. For computations of the inhibitor-Fe(110) complex, inhibitory compounds were positioned 7 Å above the top layer of the iron surface. Given that the majority of large-size organic molecules exhibit a parallel adsorption mode on metal surfaces, an initial parallel orientation was taken into consideration [24]. The following equation was used to calculate the interaction energy (E_{inter}) of each adsorption system, MeTZD-Fe(110) and MeOTZD-Fe(110):

$$E_{inter} = E_{Mol/surf} - \left(E_{surf} + E_{Mol}\right) \quad (4)$$

where E_{Mol} is the total energy of the isolated molecule, E_{surf} is the total energy of the Fe(110) slab, and $E_{Mol/surf}$ is the total energy of inhibitor-Fe(110) complexes.

2.6. Morphological Analysis

The morphological behavior of the CS surface was studied both with and without the addition of the greatest concentration of inhibitors during a 24-h exposure period using the surface morphology obtained using the SEM technique (Model-Hitachi TM-1000, recorded at a magnification of around 1000). The CS specimens were treated in the manner previously discussed in weight loss techniques.

3. Results and Discussion

3.1. Long-Term Immersion by Weight Loss Study

Long-term immersion at different temperatures ranging from 303 K to 333 K was performed to study the change in corrosion rate and inhibition efficiency before and after the addition of different concentrations of MeTZD and MeOTZD inhibitors. The effect of inhibitor concentration on the corrosion rate and inhibition performance is graphically shown in Figure 1. In Figure 1, it can be seen that the rate of CS corrosion decreases with increasing concentration, indicating that higher dosages of MeOTZD and MeTZD

inhibitors can adequately protect the CS substrates. This result is frequently ascribed to the increased number of adsorbed molecules on the steel surface, which provides better protection against corrosion. In addition, there is an improved inhibition performance of MeOTZD and MeTZD at 5×10^{-3} mol/L concentration. The comparison between the inhibition efficacy of the two inhibitors (at 5×10^{-3} mol/L) shows that the adsorption capacity of MeOTZD is superior to that of the MeTZD inhibitor. It is noticeable that the addition of the methoxy group instead of the methyl group leads to an improved adsorption ability of thiazolidinedione compounds. It is well reported that functional groups with higher electron-donating properties make a substantial difference in the adsorption of inhibitor molecules [25]. In this regard, DFT calculations were completed to evaluate the variations in the corrosion inhibition capabilities of the two studied molecules and how their molecular structures affect the adsorption strength.

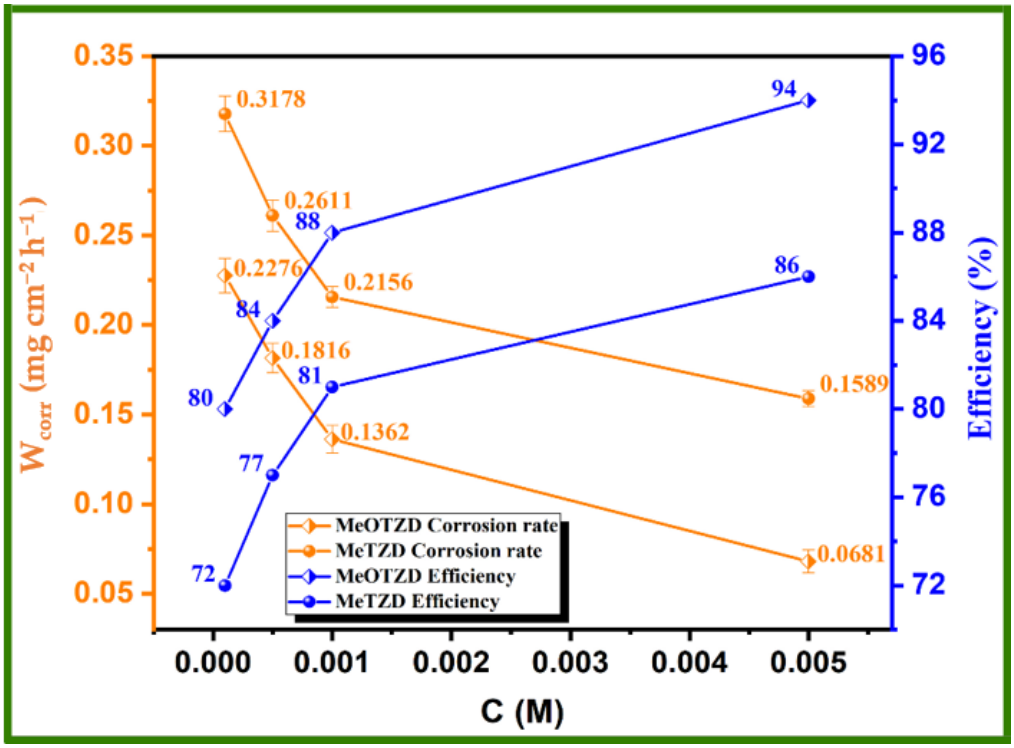

Figure 1. The relationship among corrosion rate, inhibition efficiency, and inhibitor concentration for CS after 24 h of immersion time in 1.0 mol/L HCl with MeTZD and MeOTZD at 303 K.

The corrosion process is generally considered to be significantly influenced by temperature [26–29]. The temperature effect on C_{WL} and $\eta_{WL}(\%)$ for MeOTZD and MeTZD is given in Tables 1 and 2. In addition, activation parameters were calculated and are reported in the Supplementary Material. The results in Tables 1 and 2 indicate that the inhibition efficiency decreases as temperature increases, which may indicate that the adsorbed layer of inhibitor molecules is more likely to become desorbed at high temperatures. However, at optimum conditions, inhibitors still provide higher inhibition performance at 333 K. Together, this confirms the adsorption nature of the tested molecules and their suitability for application even at higher temperatures.

Table 1. Effect of temperature on corrosion rate and inhibition efficiency in the absence and presence of different concentrations of MeOTZD compound obtained from weight loss tests.

Medium	Concentration (mol/L)	Temperature (K)	Corrosion Rate ($mg/cm^2 \times h$)	Inhibition Efficiency (%)
Blank	1.0 M HCl	303	1.135 ± 0.0121	-
		313	1.416 ± 0.0215	-
		323	1.998 ± 0.0214	-
		333	2.539 ± 0.0316	-
MeOTZD	5×10^{-3}	303	0.0681 ± 0.0034	94
		313	0.1274 ± 0.0071	91
		323	0.2197 ± 0.0098	89
		333	0.3808 ± 0.0029	85
	1×10^{-3}	303	0.1362 ± 0.0078	88
		313	0.2124 ± 0.0047	85
		323	0.3396 ± 0.0098	83
		333	0.4824 ± 0.0063	81
	5×10^{-4}	303	0.1816 ± 0.0027	84
		313	0.2549 ± 0.0067	81
		323	0.3996 ± 0.0078	80
		333	0.5586 ± 0.0088	78
	1×10^{-4}	303	0.227 ± 0.0026	80
		313	0.3115 ± 0.0043	78
		323	0.4795 ± 0.0060	76
		333	0.6855 ± 0.0079	73

Table 2. Effect of temperature on corrosion rate and inhibition efficiency in the absence and presence of different concentrations of MeTZD obtained from weight loss tests.

Medium	Concentration (mol/L)	Temperature (K)	Corrosion Rate ($mg/cm^2 \times h$)	Inhibition Efficiency (%)
Blank	1.0	303	1.135 ± 0.0121	-
		313	1.416 ± 0.0215	-
		323	1.998 ± 0.0214	-
		333	2.539 ± 0.0316	-
MeTZD	5×10^{-3}	303	0.187 ± 0.0034	83
		313	0.297 ± 0.0032	79
		323	0.539 ± 0.0067	73
		333	0.863 ± 0.0089	66
	1×10^{-3}	303	0.238 ± 0.0054	79
		313	0.368 ± 0.0035	74
		323	0.619 ± 0.0078	69
		333	0.990 ± 0.0084	61
	5×10^{-4}	303	0.295 ± 0.0098	74
		313	0.439 ± 0.0045	69
		323	0.719 ± 0.0067	64
		333	1.117 ± 0.0089	56
	1×10^{-4}	303	0.355 ± 0.0043	69
		313	0.467 ± 0.0065	65
		323	0.794 ± 0.0078	60
		333	1.193 ± 0.0085	53

3.2. PDP Measurements

PDP study was performed to characterize the cathodic and anodic responses of CS electrodes before and after the addition of MeOTZD and MeTZD inhibitors, as shown in Figure 2. Concerning the cathodic part, the presence of MeOTZD and MeTZD leads to

an insignificant modification of the cathodic slopes, showing that the reduction reaction of H^+ protons on the surface of the steel in solution is not modified by the addition of inhibitors and that it takes place according to a pure charge transfer process [30,31]. On the other hand, by inspecting anodic branches overall, one can notice an obvious decrease in anodic current densities. However, a sudden increase is observed around 300 mV/SCE. All curves remain lower than those of the blank test. At that potential, called the desorption potential, inhibitor molecules are partially desorbed from the steel surface, which makes it accessible to corrosive species, thus reducing the surface protected area [32]. Once again, this confirms the adsorption nature of selected molecules and that their adsorption is a potential-dependent phenomenon.

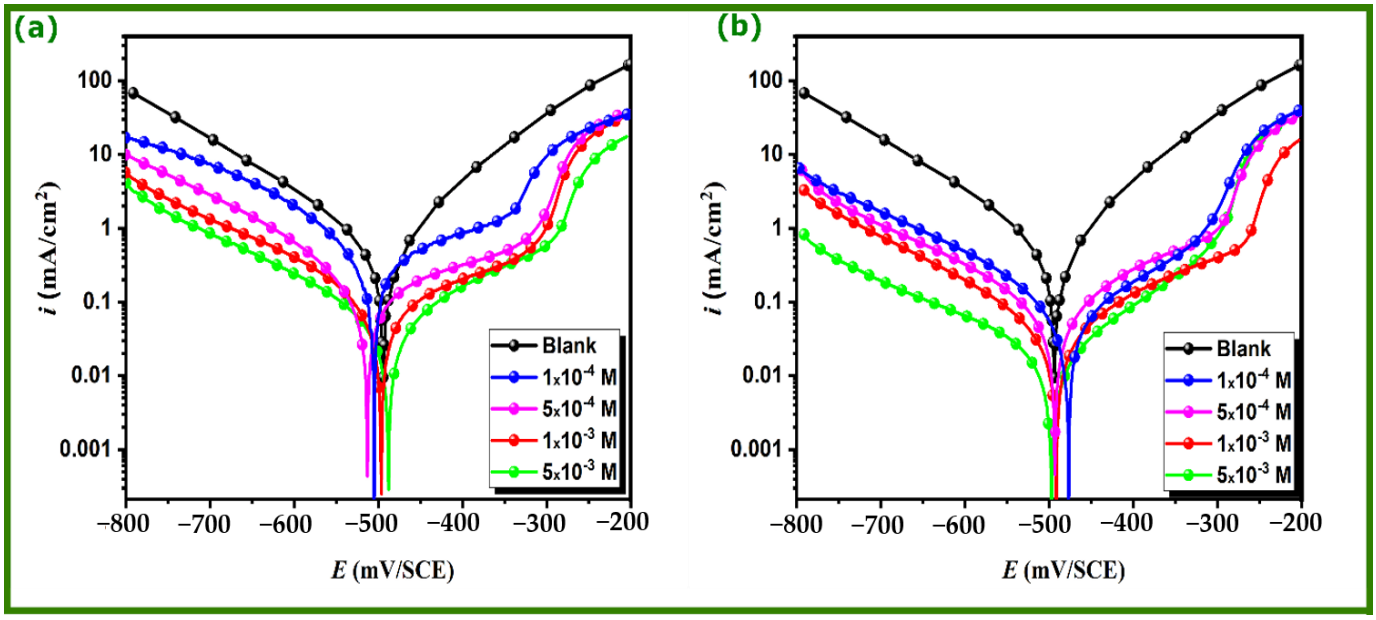

Figure 2. PDP curves of CS in 1.0 mol/L HCl solution in the absence and presence of various concentrations of (**a**) MeTZD and (**b**) MeOTZD at 303 K.

At all measured concentrations, the corrosion current density is significantly lower than the blank test. The inhibition performance of MeOTZD and MeTZD inhibitors was estimated using corrosion current according to the following equation [33]:

$$\eta_{PDP}(\%) = \frac{i^{\circ}_{corr} - i_{corr}}{i^{\circ}_{corr}} \times 100 \quad (5)$$

where i°_{corr} and i_{corr} denote the corrosion current density for uninhibited and inhibited media, respectively; the polarization parameters are listed in Table 3.

According to Table 3, the inhibitory efficacy increases with increasing inhibitor concentration until it reaches its maximum values at 5×10^{-3} mol/L for each organic compound. These findings support the outstanding corrosion inhibition characteristics of both compounds, with MeOTZD exceeding MeTZD by 8%. Additionally, MeOTZD and MeTZD inhibitors do not significantly alter the E_{corr}; hence, they function as mixed-type inhibitors, restricting both hydrogen evolution and metal dissolution reactions. The results were in good agreement with weight loss measurements. More insights about corrosion and corrosion inhibition mechanisms can be obtained from EIS tests.

Table 3. PDP parameters estimated from Tafel curves for CS in the uninhibited and inhibited 1.0 mol/L HCl solution at 303 K.

Inhibitor	Concentration (mol/L)	$-E_{corr}$ (mV vs. SCE)	$-\beta_c$ (mV dec^{-1})	i_{corr} (μAcm^{-2})	η_{PDP} (%)
Blank	1.0	496 ± 0.4	150 ± 3.5	599 ± 2.4	-
MeOTZD	5×10^{-3}	480 ± 0.6	203 ± 0.6	29.9 ± 0.8	95
	1×10^{-3}	490 ± 0.5	190 ± 0.4	59.9 ± 0.8	90
	5×10^{-4}	496 ± 0.7	183 ± 0.6	83.8 ± 0.5	86
	1×10^{-4}	501 ± 0.9	160 ± 1.2	113.8 ± 0.9	81
MeTZD	5×10^{-3}	502 ± 0.8	181 ± 1.1	77.8 ± 1.3	87
	1×10^{-3}	508 ± 1.4	170 ± 0.9	101.8 ± 0.2	83
	5×10^{-4}	480 ± 1.3	159 ± 0.6	131.8 ± 1.1	78
	1×10^{-4}	496 ± 0.5	150 ± 0.7	155.7 ± 0.6	74

3.3. Electrochemical Behavior by EIS and LPR Assessment

EIS analysis is an efficient, non-destructive method for describing an inhibitive system's corrosion inhibition properties [34,35]. Using this technique, EIS results in both Nyquist and Bode forms are represented in Figure 3. It can be seen that with increasing inhibitor concentration, Nyquist diagrams display a single capacitive loop and a larger diameter of the capacitive half loops. This indicates that the effectiveness of inhibitors depends on their concentration and that a charge transfer mechanism controls both corrosion and its inhibition [36,37]. Additionally, the adsorption of inhibitor compounds on the metal surface, which increases charge transfer resistance, can contribute to the increase in the diameter of EIS spectra. Supporting this, Bode diagrams show only one time constant at all concentrations and increased phase angle values with an increase in inhibitor concentrations.

The equivalent electrical circuit (EEC) employed to fit experimental EIS results is shown in Figure S3 [38–40]. It must be noted that the fitting quality was evaluated by the goodness of fit values (χ^2), which were of the order of 10^{-3}. An EEC model consists of a constant phase element (CPE) that is used instead of capacitance, along with solution resistance (Rs), and polarization resistance (R_p). R_p refers to the sum of all involved resistances, such as film resistance and charge transfer resistance. The capacitance (C_{dl}) is evaluated from the following equation [41]:

$$C_{dl} = \sqrt[n]{Q \times R_p^{1-n}} \tag{6}$$

where Q is a proportionality factor and n represents the surface heterogeneity.

Using R_p, the following formula is used to determine the protective capability in terms of inhibitor performance inhibition [42]:

$$\eta_{EIS}\ (\%) = \left[\frac{R_p^{inh} - R_p^{\circ}}{R_p^{inh}}\right] \times 100 \tag{7}$$

where R_p° and R_p^{inh} are the polarization resistance in the absence and presence of inhibitor compounds, respectively.

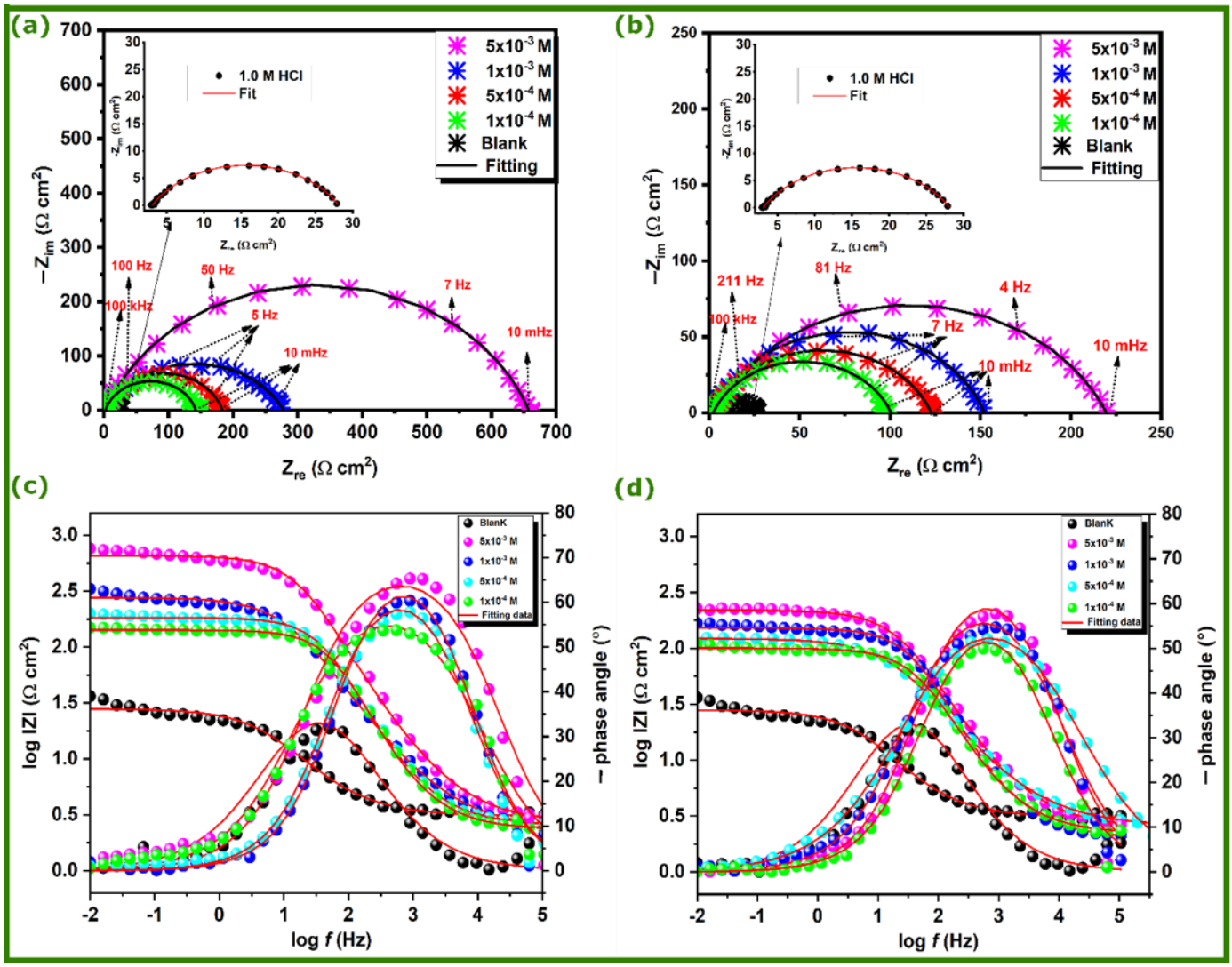

Figure 3. Nyquist and Bode diagrams of CS in 1.0 mol/L HCl solution with and without various concentrations: (**a**,**c**) MeOTZD and (**b**,**d**) MeTZD.

Table 4 regroups all parameters derived from EIS tests along with the calculated inhibition performances. It was found that the double-layer capacity (C_{dl}) and Q coefficient decrease with increasing inhibitor concentration while the polarization resistance values (R_p) increase, suggesting the modification of the double-layer behavior. It is reported that a lower capacitance value indicates a higher thickness of the protective barrier film [43], meaning a higher adsorption capability of organic compounds on the metal surface. Unsurprisingly, the corrosion inhibition performance obtained from EIS results is practically unchangeable compared to weight loss and PDP results. Structural differences between tested molecules are believed to be responsible for the observed difference in inhibition performance. An overall analysis of both molecular structures shows the presence of several active sites that are capable of participating in donor–acceptor behavior at the inhibitor/steel interface. Deep insight into the structure–activity relationship can be obtained from the first-principles DFT investigation in the theoretical sections of this work.

Table 4. EIS data estimated using impedance spectroscopy for CS corrosion in 1.0 mol/L HCl solution in the absence and presence of inhibitors at 303 K.

Inhibitor	Concentration (mol/L)	R_p (Ω cm^2)	n	$Q\times10^{-4}$ ($S^n\Omega^{-1}$ cm^{-2})	C_{dl} (μF cm^{-2})	η_{EIS} (%)
Blank	1.0	25.03 ± 1.3	0.90123 ± 0.008	1.772 ± 0.0018	97	
MeOTZD	5×10^{-3}	654.7 ± 1.9	0.78276 ± 0.009	0.220 ± 0.0043	6	96
	1×10^{-3}	275.6 ± 1.6	0.78004 ± 0.004	0.450 ± 0.0066	13	91
	5×10^{-4}	180.8 ± 1.5	0.82262 ± 0.008	0.570 ± 0.0023	21	86
	1×10^{-4}	139.7 ± 1.3	0.84478 ± 0.002	0.600 ± 0.0067	24	82
MeTZD	5×10^{-3}	217.1 ± 1.7	0.72809 ± 0.001	0.450 ± 0.0089	8	88
	1×10^{-3}	150.1 ± 0.8	0.78788 ± 0.006	0.550 ± 0.0054	15	83
	5×10^{-4}	120.2 ± 0.5	0.76825 ± 0.005	0.810 ± 0.0036	20	79
	1×10^{-4}	98.22 ± 1.4	0.79927 ± 0.009	0.910 ± 0.0078	27	74

Although all reported techniques gave similar results in terms of corrosion inhibition performance, LPR was performed for further confirmation. The results of the linear polarization resistance tests were obtained in the tested solution during 30 min of immersion. Table 5 summarizes the data of both tested molecules. The findings demonstrate that the formed film in the presence of MeOTZD and MeTZD has the highest resistance to chloride attack and that the polarization resistance improves with inhibitor concentration along with a noticeable improvement in efficiency [44,45]. The inhibitory performance of MeOTZD and MeTZD, as well as the extremely high reproducibility of the experimental procedures, demonstrate the potency of both compounds as effective inhibitors of steel in acid solution.

Table 5. Linear polarization resistance parameters of CS corrosion in 1.0 mol/L HCl solution in the absence and presence of MeTZD/MeOTZD.

System	Linear Polarization Data		
	Concentration (mol/L)	R_p (Ω cm^2)	η_{LPR} (%)
HCl	1.0	28 ± 0.9	-
MeOTZD	5×10^{-3}	731.0 ± 0.5	96
	1×10^{-3}	308.0 ± 0.8	91
	5×10^{-4}	202.1 ± 0.3	86
	1×10^{-4}	156.2 ± 1.6	82
MeTZD	5×10^{-3}	242.8 ± 0.9	88
	1×10^{-3}	167.8 ± 1.1	83
	5×10^{-4}	134.4 ± 0.6	79
	1×10^{-4}	109.8 ± 1.4	75

3.4. Adsorption Isotherm Model

Figure 4a and Figure S4 show the outcomes of the Langmuir, Freundlich, Frumkin, and Flory-Huggins adsorption isotherm models to determine which isotherms reflect the adsorption behavior of the two studied inhibitors. For the MeOTZD inhibitor, isotherms were plotted at different temperatures. Among tested models, the Langmuir adsorption isotherm (Equation (8)) was found to be more appropriate, with R^2 and slope close to 1. The Langmuir model refers to monolayer adsorption onto surfaces containing a set number of identical sites. The intercept at the origin of the linear curve C_{inh}/θ shown in Figure 4a is used to estimate the adsorption equilibrium constant (K_{ads}), which is then used to calculate the standard free energy of adsorption. The standard free energy of adsorption varies as a function of temperature, as shown graphically in Figure 4b, and this variability is used to calculate the standard enthalpy of adsorption and the standard entropy of adsorption. The kinetic adsorption characteristics for MeTZD and MeOTZD inhibitors at various

temperatures are listed in Table 6. The following equations are used to mathematically determine all of the above-mentioned characteristics [46]:

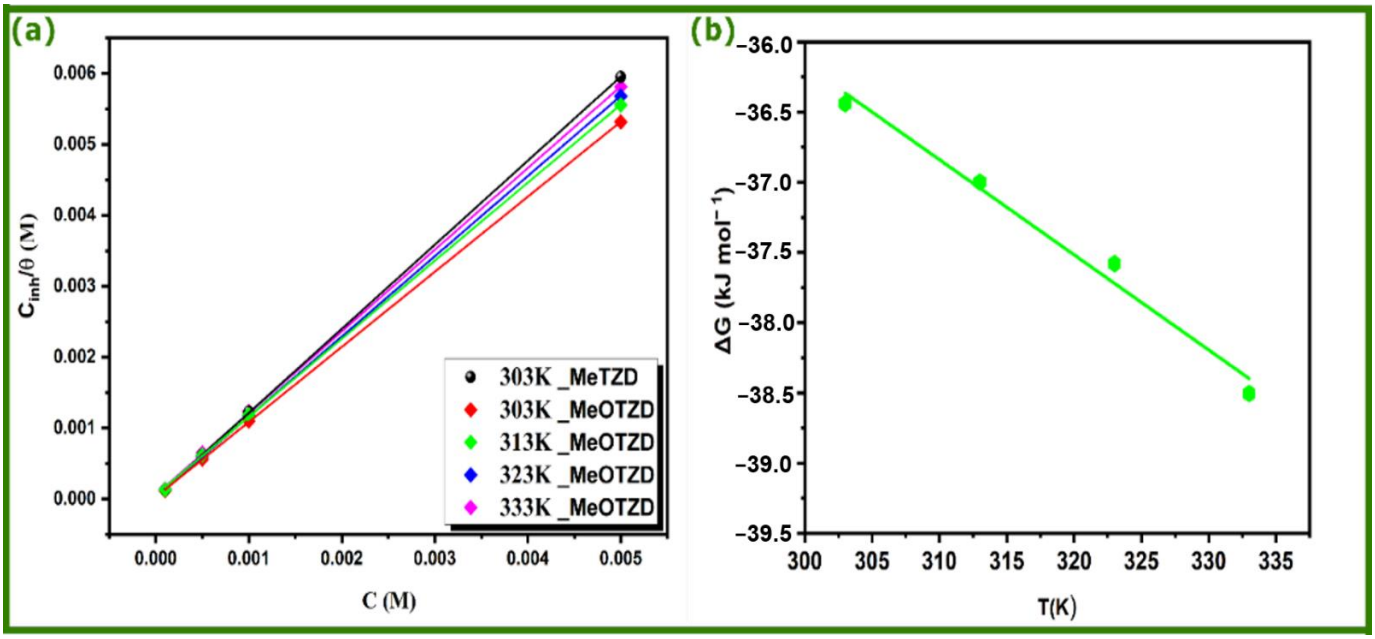

Figure 4. Langmuir adsorption isotherm plots (**a**) and regularity of the standard Gibbs free energy ΔG^{O}_{ads} value of MeOTZD vs. temperature (**b**), for CS in 1.0 mol/L HCl at different temperatures.

Table 6. Thermodynamic parameters of CS corrosion in the presence of MeOTZD and MeTZD in 1.0 mol/L HCl solution.

Inhibitor	Temperature (K)	K_{ads} (L/mol)	R^2	ΔG°_{ads} (KJ/mol)	ΔH°_{ads} (KJ/mol^{-1})	ΔS°_{ads} (J mol^{-1} K^{-1})
MeTZD	303	17,317	0.999	−34.70	-	-
MeOTZD	303	34,450	0.999	−36.44	−69.56	99
	313	17,335	0.999	−37.00		
	323	33,673	0.999	−37.58		
	333	36,948	0.999	−40.24		

$$\frac{C}{\theta} = \frac{1}{K_{ads}} + C \tag{8}$$

$$K_{ads} = \frac{1}{55.5} \times exp\left(-\frac{\Delta G^{\circ}_{ads}}{RT}\right) \tag{9}$$

$$\Delta G^{\circ}_{ads} = \Delta H^{\circ}_{ads} - T\Delta S^{\circ}_{ads} \tag{10}$$

where C denotes the concentration of compounds, K_{ads} is the constant of adsorption equilibrium, and θ refers to the surface coverage.

The adsorption process was spontaneous, and the adsorbed layer on the metal surface was stable, as suggested by the negative ΔG°_{ads} values and high values of K_{ads} [47–49]. It was found that both inhibitors exhibit ΔG°_{ads} values that are higher than −20 kJ/mol but lower than −40 kJ/mol. Additionally, the negative value of ΔH°_{ads} is found to be −69.56 kJ/mol, which indicates that heat is released during the adsorption process (exothermic process). All of these findings imply that physical and chemical interactions are involved in the adsorption of inhibitors on the steel surface [50]. The value of ΔS°_{ads} was high and positive, reflecting an increase in the disorder caused by the formation of the metal/adsorbed species combination [51].

3.5. Morphological Characterization by SEM

The impact of adding inhibitors to an HCl solution on the morphology of the CS surface is examined via SEM analysis. Inhibitors are known to prevent metals from corrosion by creating a protective barrier on their surface. Therefore, a comparison of the morphological state of the protected and unprotected steel surfaces can provide additional proof of the performance of selected compounds. Herein, given the similarity between tested compounds and their highest efficiency, MeOTZD is chosen for SEM analysis. Figure 5 shows SEM images of the CS surface after 24 h of immersion in the blank and inhibited solutions. Figure 5a depicts a heavily corroded and severely damaged metal surface. Because the steel is unprotected, corrosive species can access its surface, resulting in a deteriorated metal surface, as shown in Figure 5a. The addition of a higher concentration of MeOTZD to the HCl solution can significantly reduce its aggressiveness and therefore protect the metal from corrosion. Figure 5b demonstrates this, with a clean and smooth morphology for the protected metal. This is largely due to the formation of a protective layer on the electrode surface in contact with the inhibited corrosive solution. Hence, through a physicochemical process, the studied inhibitors are attracted to the surface of the steel to form this protective barrier.

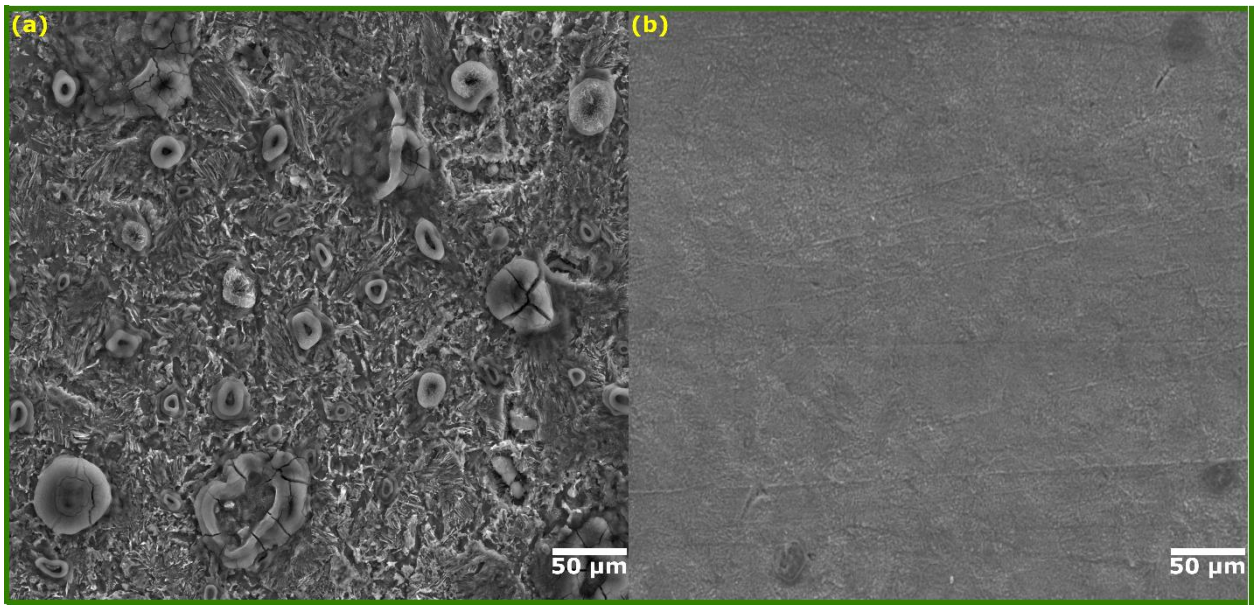

Figure 5. SEM images of the CS surface after 24 h of immersion in 1.0 mol/L HCl solution in the (**a**) absence and (**b**) presence of 5×10^{-3} M of MeOTZD.

3.6. First-Principles DFT Evaluations

3.6.1. Adsorption Configuration and Interaction Energy

The physical and chemical adsorption process was highlighted as the main corrosion inhibition mechanism by experimental results and related analyses. This conclusion can be subjected to more investigation by modeling the interactions between inhibitor molecules and iron surfaces using first-principles DFT calculations. In comparison to widely reported quantum chemical calculations that rely on comparing some global reactivity descriptors without taking the metal into account, first-principle DFT calculations have emerged as a robust approach to obtaining physical insights that experiments and other theoretical techniques cannot provide [52]. Figure 6 shows the most stable adsorption geometries of the evaluated molecules on the Fe(110) surface. Because large-sized organic molecules typically assume a parallel arrangement on metal surfaces, only the parallel adsorption mode has been taken into consideration.

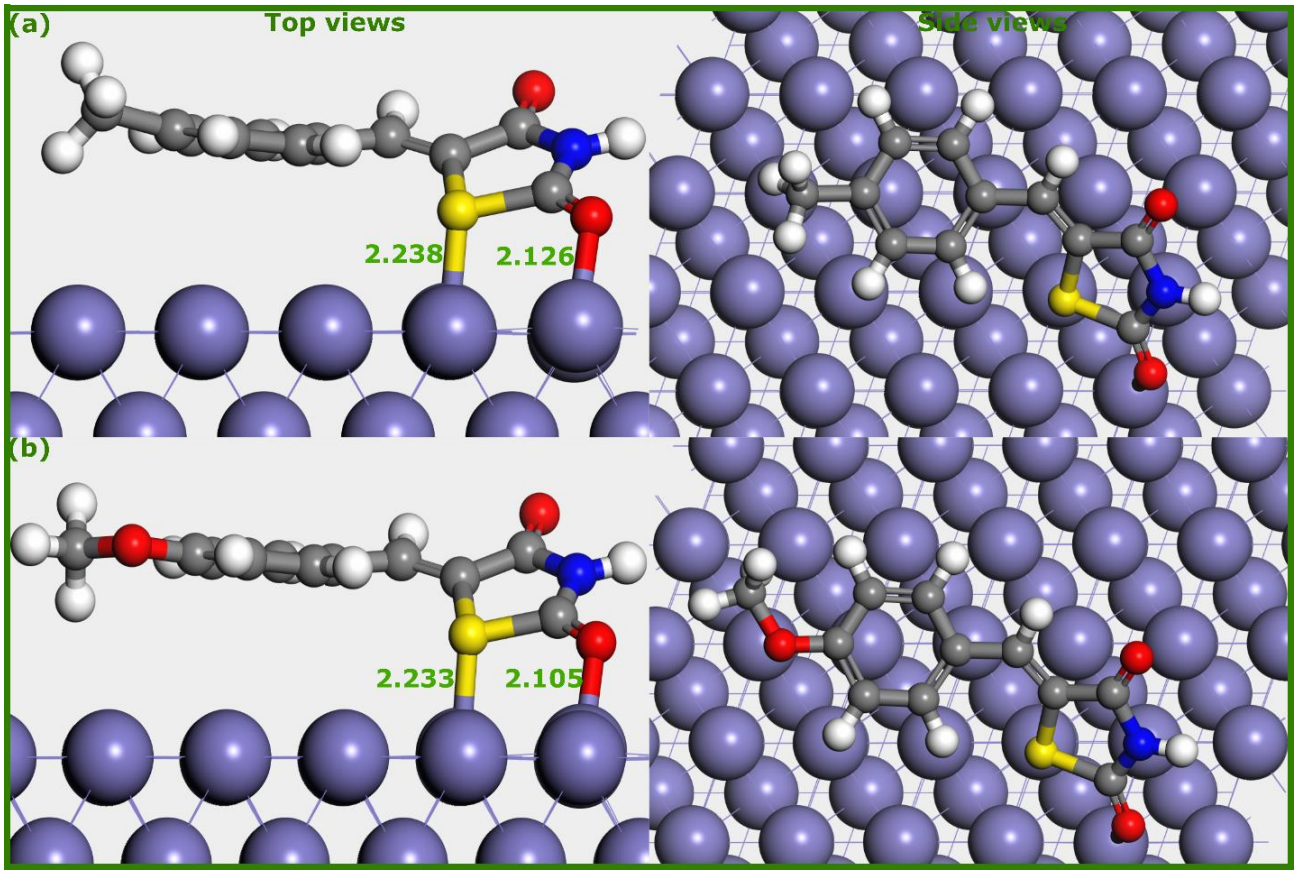

Figure 6. Optimized adsorption geometries of (**a**) MeTZD and (**b**) MeOTZD on Fe(110) surface obtained via first-principles DFT calculations. Optimized bond lengths are in Å.

From a careful inspection of Figure 6, one can observe that both molecules have a nearly flat disposition over the Fe(110) surface. In this geometry, molecules bond to Fe-atoms through the oxygen of the carbonyl group and sulfur atoms. The other parts, especially the phenyl rings, are parallelly adsorbed but without bond formation. The distance lengths of the formed bonds are in the order of 2.10 and 2.23 Å. The thiazolidinedione moiety is very rich in electrons with available free electron pairs on heteroatoms, so it is expected to build a strong affinity towards iron atoms. In general, the covalent radii sum of Fe-S ($r_S + r_{Fe}$) and Fe-O ($r_O + r_{Fe}$) is 2.37 Å and 1.98 Å, respectively [53]. This signifies that formed bonds between S and O atoms and the iron surface are within the sum of the covalent radii. Thus, it is possible to infer that both molecules are chemically adsorbed over the surface of Fe(110).

However, insights about the adsorption strength of each molecule cannot be obtained via visual inspection. Thus, the interaction energies of each adsorption system are calculated to determine which molecule has a strong adsorption power. The interaction energies for MeOTZD-Fe(110) and MeTZD-Fe(110) were −1.11 and −1.04 eV, respectively. This means that both molecules have favorable adsorption ability; however, MeOTZD outperforms MeTZD by −0.07 eV [24]. This is, as stated before, mostly due to the high electron-donating power of the methoxyphenyl group compared to the methylphenyl group. Still, despite this difference, it is fair to say that both molecules have excellent adsorption properties thanks to the presence of several active sites in the thiazolidinedione moiety. Such functional groups can significantly improve the adsorption capacity of inhibitor molecules [54].

3.6.2. Projected Density of States (PDOS)

The adsorption systems discussed in the previous section can be well interpreted by analyzing the projected density of states of interacted atoms in isolated and adsorbed

forms. This is especially helpful in identifying the mechanism by which molecules interact with the metal surface [55]. Therefore, the density of states analysis is carried out for the investigated molecules. Figure 7 (MeTZD) and Figure 8 (MeOTZD) show the results of PDOS calculations for iron, isolated molecules, and adsorbed inhibitor molecules.

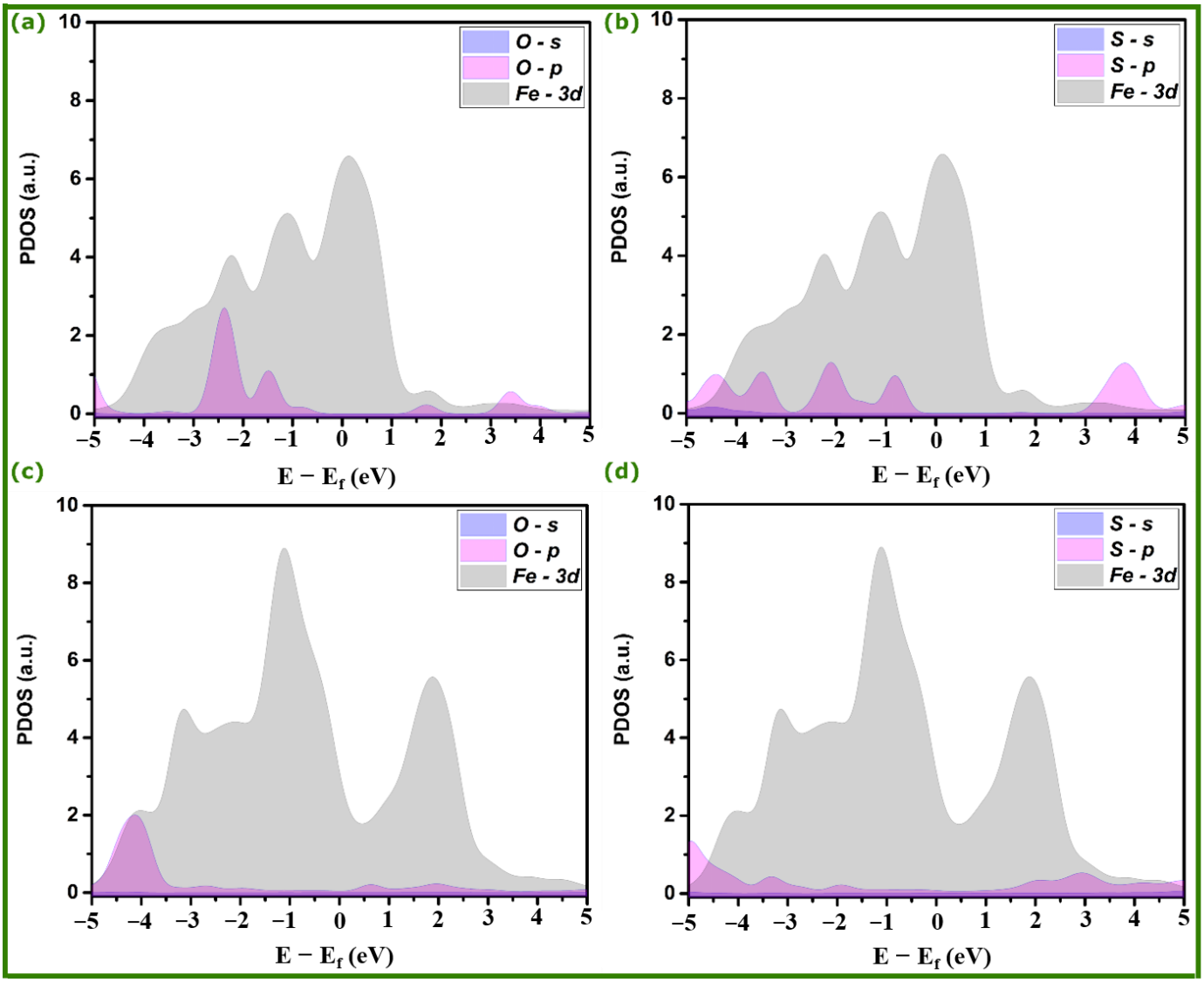

Figure 7. PDOS for MeTZD molecules adsorbed on Fe(110) surface and the Fe atoms beneath them. (**a**,**b**) isolated inhibitor molecule 7 Å above iron surface and (**c**,**d**) optimized adsorption geometry of molecule.

Given that all of the Fe 3d states are included within this energy range, the chemical states are examined in the region of −5 to 5 eV [56,57]. The chemical states of adsorbed S and O atoms are considered for a precise interpretation of the results. The molecular states of the S and O atoms, which are located in the s and p orbitals, are displayed in the top panels of Figures 7 and 8. In both cases, molecular states are in the form of sharper, well-structured peaks. As these peaks are located in the same energy range as Fe 3d bands, they are expected to hybridize during adsorption on the iron surface. In fact, this is the case when we observe PDOS results in the bottom panel of Figures 7 and 8. In contrast to their states in isolated forms, the results demonstrate that the peaks in question become unstructured and significantly decrease. This means that S and O atoms participate in strong charge transfers and binding with vacant d-orbitals of iron [24]. In this scenario,

given the fact that chemisorption is the strongest adsorption mechanism, these atoms are the most responsible for the adsorption of molecules on the steel surface, thus improving corrosion inhibition performance. Thanks to the free electron pairs on these atoms, a charge transfer with the vacant d-orbitals of iron is likely to happen easily when interacting with the iron surface. In addition, structural differences are confirmed to be responsible for the adsorption strength of selected molecules, since their adsorption geometries are similar. The additional electron-donating methoxyphenyl group increases the interactive power of MeOTZD, and therefore its corrosion inhibition performance.

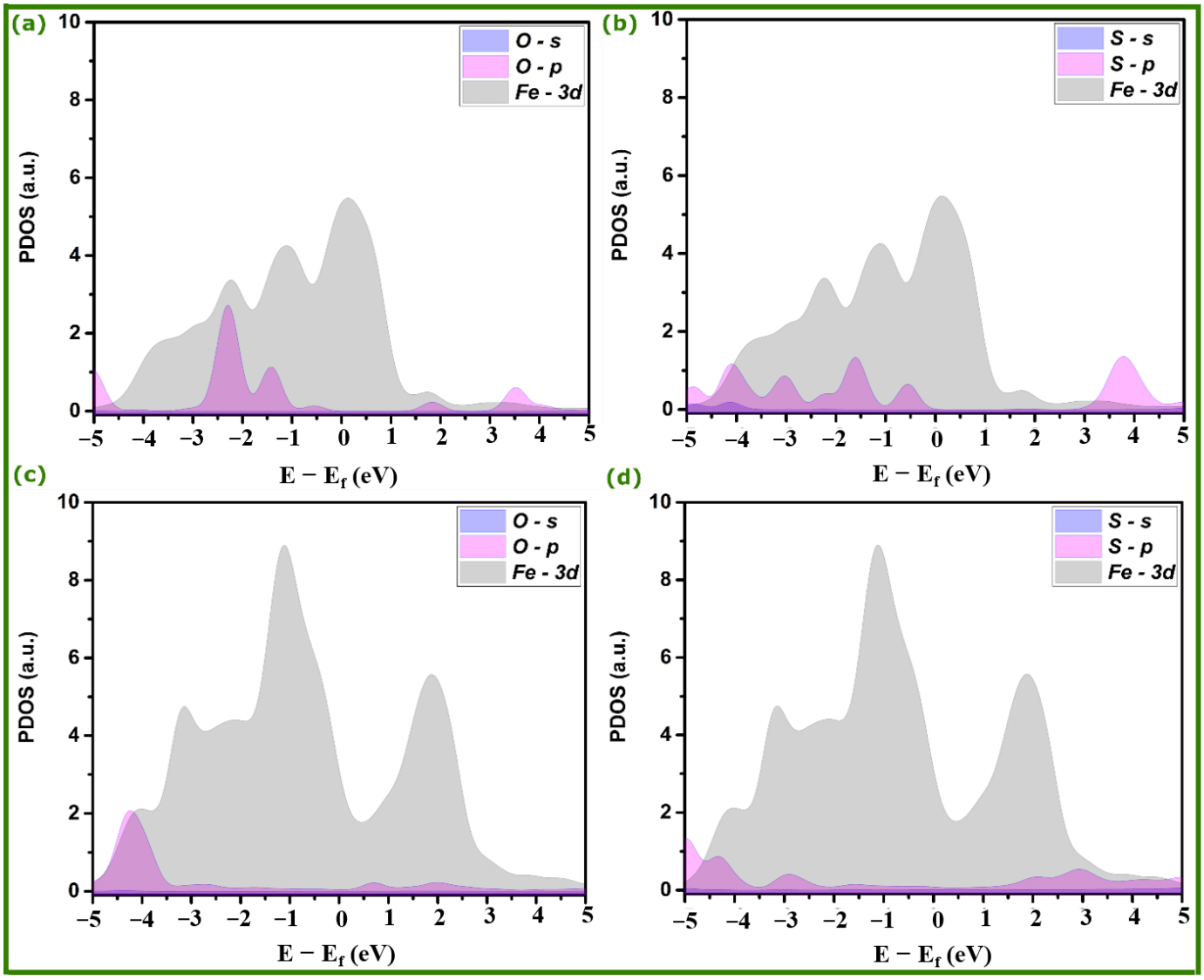

Figure 8. PDOS for MeOTZD molecules adsorbed on Fe(110) surface and the Fe atoms beneath them. (**a**,**b**) isolated inhibitor molecule 7 Å above iron surface and (**c**,**d**) optimized adsorption geometry of molecule.

3.7. Adsorption Mechanism of Adsorbed Molecules

Based on experimental and theoretical insights, the adsorption mechanism of the interaction between selected molecules and the iron surface can be proposed, as shown in Figure 9. It has generally been reported that organic molecules having heteroatoms in their molecular structures are protonated easily when immersed in 1.0 mol/L HCl [58,59]. On the other hand, the steel surface was found to have a positive charge in similar conditions [58,59]. In this situation, and due to the electrostatic repulsion, molecules can

only be adsorbed through pre-adsorbed chlorine ions, which change steel's interfacial charge to negative. This step is necessary for a successful corrosion inhibition process by organic molecules, and it is called the physisorption process. Chemical bonding and charge transfer of free electron pairs on O and S atoms to unoccupied d-orbitals of iron are strongly anticipated as molecules approach the steel surface. This is the main adsorption step that is believed to be responsible for the effectiveness of an organic corrosion inhibitor. In addition, the accumulation of charges on the CS surface can prevent the transfer of charges from the steel surface to the inhibitor molecules' anti-bonding orbitals, which is called the retro-donation process. These conclusions seem reasonable considering the experimental and theoretical results, which both suggest the adsorption of molecules on the steel surface through physical and chemical interactions and considering previously published results [60–62].

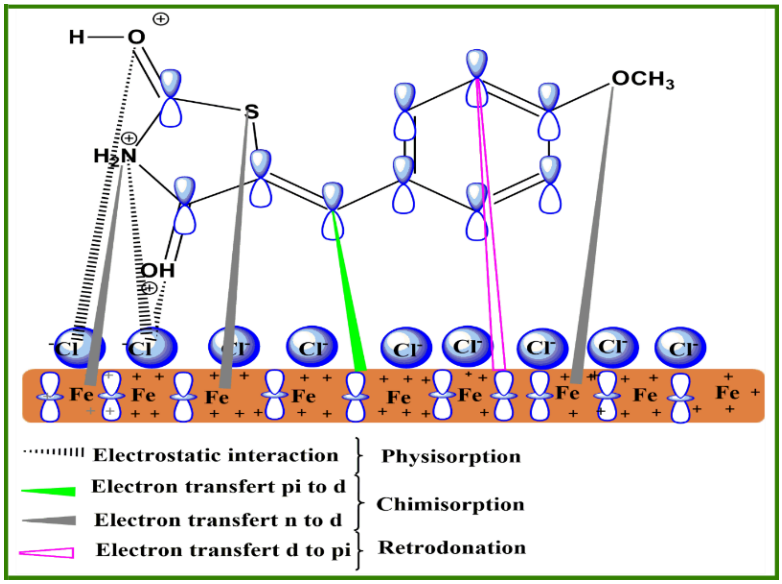

Figure 9. Pictorial representation of adsorption mechanism of MeOTZD on CS surface in 1 mol/L HCl.

4. Conclusions

In the present study, the electrochemical behavior and adsorption properties of two thiazolidinedione derivatives were evaluated to explore their ability to prevent corrosion of carbon steel in HCl solution. An experimental investigation was carried out by electrochemical techniques along with weight loss tests, while useful physical insights about inhibitors' adsorption were obtained by first-principles DFT calculations. Considering both experimental and theoretical evaluations, MeOTZD and MeTZD were found effective against steel corrosion in the HCl medium. With increasing inhibitor concentration, the inhibition performance of the two studied inhibitors improves, showing exceptional protective properties (the maximum performance of MeOTZD and MeTZD is 96% and 88% at 5×10^{-3} mol/L, respectively). The two tested inhibitors had a mixed inhibitory effect, blocking both anodic and cathodic corrosion reactions and reducing the corrosion current density compared to the blank solution. Electrochemical data revealed that thiazolidinedione derivatives significantly improved the polarization resistance and modified the double-layer behavior due to their adsorption on the steel surface. The adsorption was found to follow the Langmuir isotherm model. Furthermore, SEM analysis showed that inhibitors' addition to the HCl solution created a protective layer that prevented the CS surface from corrosion. First-principles DFT calculations revealed the formation of covalent bonds between S and O atoms of molecules and Fe-atoms, which was confirmed by PDOS results. The findings of the present work can shed more light on the application of thiazolidinedione derivatives in the corrosion protection of metals.

Supplementary Materials: The following supporting information can be downloaded at: https://www.mdpi.com/article/10.3390/met12101598/s1, Figure S1: The variation of open circuit potential as function of time of MeOTZD (a) and MeTZD (b), Figure S2: Arrhenius (a) and transition state (b) plots for corrosion inhibition of carbon steel in absence and presence of different concentrations of MeOTZD in 1.0 M HCl, Figure S3: Equivalent circuit model applied to fit and simulate the impedance data, Figure S4: Isotherm plots for carbon steel in 1.0 M HCl medium at 303 K containing different concentrations of MeOTZD and MeTZD. Table S1: MeOTZD activation parameters.

Author Contributions: Conceptualization, methodology, writing—original draft, A.C., M.C. and H.L.; formal analysis, A.H.A.-M.; data curation, F.Z.T.; investigation and resources, R.S., K.K., K.B. and I.H.A.; visualization and editing, Y.G.K. and H.L. All authors have read and agreed to the published version of the manuscript.

Funding: This work was supported by the Fundamental-Core National Project of the National Research Foundation (NRF) funded by the Ministry of Science and ICT, Republic of Korea (2022R1F1A1072739). The authors extend their appreciation to the Deanship of Scientific Research at King Khalid University for funding this work through the research groups program under grant number R.G.P.2/84/43.

Data Availability Statement: Raw data used for this work is part of ongoing works and cannot be shared at this time.

Conflicts of Interest: The authors declare no conflict of interest.

References

1. Aboelnga, M.M.; Awad, M.K.; Gauld, J.W.; Mustafa, M.R. An assessment to evaluate the validity of different methods for the description of some corrosion inhibitors. *J. Mol. Model.* **2014**, *20*, 1–17. [CrossRef] [PubMed]
2. Sanaei, Z.; Ramezanzadeh, M.; Bahlakeh, G.; Ramezanzadeh, B. Use of Rosa canina fruit extract as a green corrosion inhibitor for mild steel in 1M HCl solution: A complementary experimental, molecular dynamics and quantum mechanics investigation. *J. Ind. Eng. Chem.* **2019**, *69*, 18–31. [CrossRef]
3. Ramezanzadeh, M.; Bahlakeh, G.; Sanaei, Z.; Ramezanzadeh, B. Corrosion inhibition of mild steel in 1 M HCl solution by ethanolic extract of eco-friendly Mangifera indica (mango) leaves: Electrochemical, molecular dynamics, Monte Carlo and ab initio study. *Appl. Surf. Sci.* **2019**, *463*, 1058–1077. [CrossRef]
4. Nikoo, S.Z.; Shockravi, A.; Ghartavol, H.M.; Halimehjani, A.Z.; Ostadrahimi, M.; Mirhosseini, S.M.; Behzadi, H.; Ghorbani, M. A study of glycine-based dithiocarbamates as effective corrosion inhibitors for cold rolled carbon steel in HCl solutions. *Surf. Interfaces* **2020**, *21*, 100751. [CrossRef]
5. Tiwari, N.; Mitra, R.K.; Yadav, M. Corrosion protection of petroleum oil well/tubing steel using thiadiazolines as efficient corrosion inhibitor: Experimental and theoretical investigation. *Surf. Interfaces* **2021**, *22*, 100770. [CrossRef]
6. Jafarpour, H.; Aghaei, H.; Litvin, V.; Ashena, R. Experimental optimization of a recently developed matrix acid stimulation technology in heterogeneous carbonate reservoirs. *J. Pet. Sci. Eng.* **2021**, *196*, 108100. [CrossRef]
7. Solomon, M.M.; Umoren, S.A.; Quraishi, M.A.; Tripathy, D.B.; Abai, E.J. Effect of akyl chain length, flow, and temperature on the corrosion inhibition of carbon steel in a simulated acidizing environment by an imidazoline-based inhibitor. *J. Pet. Sci. Eng.* **2020**, *187*, 106801. [CrossRef]
8. Hajjaji, F.E.; Salim, R.; Taleb, M.; Benhiba, F.; Rezki, N.; Chauhan, D.S.; Quraishi, M.A. Pyridinium-based ionic liquids as novel eco-friendly corrosion inhibitors for mild steel in molar hydrochloric acid: Experimental & computational approach. *Surf. Interfaces* **2021**, *22*, 100881. [CrossRef]
9. Fernandes, C.M.; Faro, L.V.; Pina, V.G.S.S.; de Souza, M.C.B.V.; Boechat, F.C.S.; de Souza, M.C.; Briganti, M.; Totti, F.; Ponzio, E.A. Study of three new halogenated oxoquinolinecarbohydrazide N-phosphonate derivatives as corrosion inhibitor for mild steel in acid environment. *Surf. Interfaces* **2020**, *21*, 100773. [CrossRef]
10. Damej, M.; Kaya, S.; Ibrahimi, B.E.; Lee, H.-S.; Molhi, A.; Serdaroğlu, G.; Benmessaoud, M.; Ali, I.H.; Hajjaji, S.E.; Lgaz, H. The corrosion inhibition and adsorption behavior of mercaptobenzimidazole and bis-mercaptobenzimidazole on carbon steel in 1.0 M HCl: Experimental and computational insights. *Surf. Interfaces* **2021**, *24*, 101095. [CrossRef]
11. Jodeh, S.; Larouj, M.; Lgaz, H.; Salghi, R.; Oudda, H.; Chetouani, A. Inhibitive Action of Sodium tetrafluoroborate on the Corrosion of Carbon Steel in Hydrochloric Acid Medieum. *Moroc. J. Chem.* **2016**, *4*, 425–436.
12. Larouj, M.; Lgaz, H.; Salghi, R.; Jodeh, S.; Messali, M.; Zougagh, M.; Oudda, H.; Chetouani, A. Effect of chlorine group position on adsorption behavior and corrosion inhibition of Chlorobenzylideneamino-5-methyl-2,4-dihydro-1,2,4-triazole-3-thione Schiff bases: Experimental study. *Moroc. J. Chem.* **2016**, *4*, 567–583.
13. Nanjan, M.J.; Mohammed, M.; Kumar, B.R.P.; Chandrasekar, M.J.N. Thiazolidinediones as antidiabetic agents: A critical review. *Bioorganic Chem.* **2018**, *77*, 548–567. [CrossRef]
14. Lebovitz, H.E. Thiazolidinediones: The forgotten diabetes medications. *Curr. Diab. Rep.* **2019**, *19*, 1–13. [CrossRef] [PubMed]

15. Mendonça, G.L.; Costa, S.N.; Freire, V.N.; Casciano, P.N.; Correia, A.N.; de Lima-Neto, P. Understanding the Corrosion Inhibition of Carbon Steel and Copper in Sulphuric Acid Medium by Amino Acids Using Electrochemical Techniques Allied to Molecular Modelling Methods. *Corros. Sci.* **2017**, *115*, 41–55. [CrossRef]
16. Zhang, D.; Gao, L.; Zhou, G. Inhibition of Copper Corrosion by Bis-(1-Benzotriazolymethylene)-(2,5-Thiadiazoly)-Disulfide in Chloride Media. *Appl. Surf. Sci.* **2004**, *225*, 287–293. [CrossRef]
17. Yadav, M.; Behera, D.; Kumar, S.; Yadav, P. Experimental and Quantum Chemical Studies on Corrosion Inhibition Performance of Thiazolidinedione Derivatives for Mild Steel in Hydrochloric Acid Solution. *Chem. Eng. Commun.* **2015**, *202*, 303–315. [CrossRef]
18. Lgaz, H.; Saha, S.K.; Lee, H.-S.; Kang, N.; Thari, F.Z.; Karrouchi, K.; Salghi, R.; Bougrin, K.; Ali, I.H. Corrosion Inhibition Properties of Thiazolidinedione Derivatives for Copper in 3.5 wt.% NaCl Medium. *Metals* **2021**, *11*, 1861. [CrossRef]
19. Thari, F.Z.; Tachallait, H.; el Alaoui, N.-E.; Talha, A.; Arshad, S.; Álvarez, E.; Karrouchi, K.; Bougrin, K. Ultrasound-assisted one-pot green synthesis of new N- substituted-5-arylidene-thiazolidine-2,4-dione-isoxazoline derivatives using NaCl/Oxone/Na_3PO_4 in aqueous media. *Ultrason. Sonochemistry* **2020**, *68*, 105222. [CrossRef]
20. Chen, Z.; Huang, L.; Zhang, G.; Qiu, Y.; Guo, X. Benzotriazole as a Volatile Corrosion Inhibitor during the Early Stage of Copper Corrosion under Adsorbed Thin Electrolyte Layers. *Corros. Sci.* **2012**, *65*, 214–222. [CrossRef]
21. Singh, P.; Ebenso, E.E.; Olasunkanmi, L.O.; Obot, I.B.; Quraishi, M. Electrochemical, theoretical, and surface morphological studies of corrosion inhibition effect of green naphthyridine derivatives on mild steel in hydrochloric acid. *J. Phys. Chem. C.* **2016**, *120*, 3408–3419. [CrossRef]
22. Lutts, A.; Gielen, P. The precise determination of the lattice parameter of α-iron and some of its alloys. *J. Appl. Crystallogr.* **1971**, *4*, 242–250. [CrossRef]
23. Guo, L.; Obot, I.B.; Zheng, X.; Shen, X.; Qiang, Y.; Kaya, S.; Kaya, C. Theoretical insight into an empirical rule about organic corrosion inhibitors containing nitrogen, oxygen, and sulfur atoms. *Appl. Surf. Sci.* **2017**, *406*, 301–306. [CrossRef]
24. Guo, L.; Qi, C.; Zheng, X.; Zhang, R.; Shen, X.; Kaya, S. Toward understanding the adsorption mechanism of large size organic corrosion inhibitors on an Fe(110) surface using the DFTB method. *RSC Adv.* **2017**, *7*, 29042–29050. [CrossRef]
25. Verma, C.; Olasunkanmi, L.O.; Ebenso, E.E.; Quraishi, M.A. Substituents effect on corrosion inhibition performance of organic compounds in aggressive ionic solutions: A review. *J. Mol. Liq.* **2018**, *251*, 100–118. [CrossRef]
26. Khadom, A.A. Effect of temperature on corrosion inhibition of copper-nickel alloy by tetraethylenepentamine under flow conditions. *J. Chil. Chem. Soc.* **2014**, *59*, 2545–2549. [CrossRef]
27. Desimone, M.; Gordillo, G.; Simison, S.N. The effect of temperature and concentration on the corrosion inhibition mechanism of an amphiphilic amido-amine in CO2 saturated solution. *Corros. Sci.* **2011**, *53*, 4033–4043. [CrossRef]
28. Kairi, N.I.; Kassim, J. The effect of temperature on the corrosion inhibition of mild steel in 1 M HCl solution by Curcuma longa extract. *Int. J. Electrochem. Sci.* **2013**, *8*, 7138–7155.
29. Elawady, Y.; Ahmed, A.I. Effect of Temperature & Inhibitors on the Corrosion of Aluminium in 2NHCI Solution: A Kinetic Study. *Indian J. Chem.* **1985**, *24A*, 601–602.
30. Kubba, R.M.; Alag, A.S. Experimental and Theoretical Evaluation of new Quinazolinone Derivative as Organic Corrosion Inhibitor for Carbon Steel in 1M HCl Solution. *Int. J. Sci. Res.* **1832**, *6*, 1643.
31. Lgaz, H.; Salghi, R.; Jodeh, S.; Hammouti, B. Effect of clozapine on inhibition of mild steel corrosion in 1.0 M HCl medium. *J. Mol. Liq.* **2017**, *225*, 271–280. [CrossRef]
32. Zhang, W.; Li, H.-J.; Wang, Y.; Liu, Y.; Wu, Y.-C. Adsorption and corrosion inhibition properties of pyridine-2-aldehyde-2-quinolylhydrazone for Q235 steel in acid medium: Electrochemical, thermodynamic, and surface studies. *Mater. Corros.* **2018**, *69*, 1638–1648. [CrossRef]
33. Chaouiki, A.; Lgaz, H.; Salghi, R.; Gaonkar, S.L.; Bhat, K.S.; Jodeh, S.; Toumiat, K.; Oudda, H. New Benzohydrazide Derivative as Corrosion Inhibitor for Carbon Steel in a 1.0 M HCl Solution: Electrochemical, DFT and Monte Carlo Simulation Studies. *Port. Electrochimica Acta.* **2019**, *37*, 147–165. [CrossRef]
34. Selatnia, I.; Sid, A.; Benahmed, M.; Debbih, O.D.; Ozturk, T.; Gherraf, N. Synthesis and Characterization of a Bis-Pyrazoline Derivative as Corrosion Inhibitor for A283 Carbon Steel in 1M HCl: Electrochemical, Surface, DFT and MD Simulation Studies. *Prot. Met. Phys. Chem. Surf.* **2018**, *54*, 1182–1193. [CrossRef]
35. Cao, Z.; Tang, Y.; Cang, H.; Xu, J.; Lu, G.; Jing, W. Novel benzimidazole derivatives as corrosion inhibitors of mild steel in the acidic media. Part II: Theoretical studies. *Corros. Sci.* **2014**, *83*, 292–298. [CrossRef]
36. Macdonald, J.R. Impedance spectroscopy and its use in analyzing the steady-state AC response of solid and liquid electrolytes. *J. Electroanal. Chem. Interfacial Electrochem.* **1987**, *223*, 25–50. [CrossRef]
37. Avdeev, Y.G.; Kuznetsov, Y.I.; Buryak, A.K. Inhibition of steel corrosion by unsaturated aldehydes in solutions of mineral acids. *Corros. Sci.* **2013**, *69*, 50–60. [CrossRef]
38. Ansari, K.R.; Quraishi, M.A.; Singh, A. Pyridine derivatives as corrosion inhibitors for N80 steel in 15% HCl: Electrochemical, surface and quantum chemical studies. *Measurement* **2015**, *76*, 136–147. [CrossRef]
39. Chong, A.L.; Mardel, J.I.; MacFarlane, D.R.; Forsyth, M.; Somers, A.E. Synergistic corrosion inhibition of mild steel in aqueous chloride solutions by an imidazolinium carboxylate salt. *ACS Sustain. Chem. Eng.* **2016**, *4*, 1746–1755. [CrossRef]
40. Abdallah, Z.A.; Ahmed, M.S.M.; Saleh, M. Organic synthesis and inhibition action of novel hydrazide derivative for mild steel corrosion in acid solutions. *Mater. Chem. Phys.* **2016**, *174*, 91–99. [CrossRef]

41. Zhang, Z.; Tian, N.C.; Huang, X.D.; Shang, W.; Wu, L. Synergistic inhibition of carbon steel corrosion in 0.5 M HCl solution by indigo carmine and some cationic organic compounds: Experimental and theoretical studies. *RSC Adv.* **2016**, *6*, 22250–22268. [CrossRef]
42. Gholami, M.; Danaee, I.; Maddahy, M.H.; RashvandAvei, M. Correlated ab initio and electroanalytical study on inhibition behavior of 2-mercaptobenzothiazole and its thiole–thione tautomerism effect for the corrosion of steel (API 5L X52) in sulphuric acid solution. *Ind. Eng. Chem. Res.* **2013**, *52*, 14875–14889. [CrossRef]
43. Hirschorn, B.; Orazem, M.E.; Tribollet, B.; Vivier, V.; Frateur, I.; Musiani, M. Determination of effective capacitance and film thickness from constant-phase-element parameters. *Electrochimica Acta* **2010**, *55*, 6218–6227. [CrossRef]
44. Aoun, S.B. On the corrosion inhibition of carbon steel in 1 M HCl with a pyridinium-ionic liquid: Chemical, thermodynamic, kinetic and electrochemical studies. *RSC Adv.* **2017**, *7*, 36688–36696. [CrossRef]
45. Bayol, E.; Gürten, A.; Dursun, M.; Kayakirilmaz, K. Adsorption behavior and inhibition corrosion effect of sodium carboxymethyl cellulose on mild steel in acidic medium. *Acta Phys. Chim. Sin.* **2008**, *24*, 2236–2243. [CrossRef]
46. Myung, N.V.; Park, D.-Y.; Yoo, B.-Y.; Sumodjo, P.T. Development of electroplated magnetic materials for MEMS. *J. Magn. Magn. Mater.* **2003**, *265*, 189–198. [CrossRef]
47. Olasunkanmi, L.O.; Obot, I.B.; Ebenso, E.E. Adsorption and corrosion inhibition properties of N-{n-[1-R-5-(quinoxalin-6-yl)-4, 5-dihydropyrazol-3-yl] phenyl} methanesulfonamides on mild steel in 1 M HCl: Experimental and theoretical studies. *RSC Adv.* **2016**, *6*, 86782–86797. [CrossRef]
48. Saha, S.K.; Dutta, A.; Ghosh, P.; Sukul, D.; Banerjee, P. Adsorption and corrosion inhibition effect of Schiff base molecules on the mild steel surface in 1 M HCl medium: A combined experimental and theoretical approach. *Phys. Chem. Chem. Phys.* **2015**, *17*, 5679–5690. [CrossRef]
49. Fouda, A.; Diab, M.; Fathy, S. Role of Some Organic Compounds as Corrosion Inhibitors for 316L Stainless Steel in 1 M HCl. *Int. J. Electrochem. Sci.* **2017**, *12*, 347–362. [CrossRef]
50. Chafiq, M.; Chaouiki, A.; Al-Hadeethi, M.R.; Salghi, R.; Ismat, H.A.; Shaaban, K.M.; Chung, I.-M. A joint experimental and theoretical investigation of the corrosion inhibition behavior and mechanism of hydrazone derivatives for mild steel in HCl solution. *Colloids Surf. A Physicochem. Eng. Asp.* **2021**, *610*, 125744. [CrossRef]
51. Singh, P.; Srivastava, V.; Quraishi, M. Novel quinoline derivatives as green corrosion inhibitors for mild steel in acidic medium: Electrochemical, SEM, AFM, and XPS studies. *J. Mol. Liq.* **2016**, *216*, 164–173. [CrossRef]
52. Kokalj, A. On the alleged importance of the molecular electron-donating ability and the HOMO–LUMO gap in corrosion inhibition studies. *Corros. Sci.* **2021**, *180*, 109016. [CrossRef]
53. Kovačević, N.; Kokalj, A. Chemistry of the interaction between azole type corrosion inhibitor molecules and metal surfaces. *Mater. Chem. Phys.* **2012**, *137*, 331–339. [CrossRef]
54. Singh, A.; Ansari, K.R.; Haque, J.; Dohare, P.; Lgaz, H.; Salghi, R.; Quraishi, M.A. Effect of electron donating functional groups on corrosion inhibition of mild steel in hydrochloric acid: Experimental and quantum chemical study. *J. Taiwan Inst. Chem. Eng.* **2018**, *82*, 233–251. [CrossRef]
55. Kumar, D.; Jain, N.; Jain, V.; Rai, B. Amino acids as copper corrosion inhibitors: A density functional theory approach. *Appl. Surf. Sci.* **2020**, *514*, 145905. [CrossRef]
56. Kumar, D.; Jain, V.; Rai, B. Unravelling the mechanisms of corrosion inhibition of iron by henna extract: A density functional theory study. *Corros. Sci.* **2018**, *142*, 102–109. [CrossRef]
57. Özcan, M.; Toffoli, D.; Üstünel, H.; Dehri, İ. Insights into surface–adsorbate interactions in corrosion inhibition processes at the molecular level. *Corros. Sci.* **2014**, *80*, 482–486. [CrossRef]
58. Solmaz, R. Investigation of corrosion inhibition mechanism and stability of Vitamin B1 on mild steel in 0.5 M HCl solution. *Corros. Sci.* **2014**, *81*, 75–84. [CrossRef]
59. Solmaz, R.; Şahin, E.A.; Döner, A.; Kardaş, G. The investigation of synergistic inhibition effect of rhodanine and iodide ion on the corrosion of copper in sulphuric acid solution. *Corros. Sci.* **2011**, *53*, 3231–3240. [CrossRef]
60. Wu, Y.; Guo, L.; She, Y. Insight on the corrosion inhibition performance of psidium guajava linn leaves extract. *J. Mol. Liq.* **2022**, *346*, 117858. [CrossRef]
61. Sharma, S.; Kumar, A. Recent advances in metallic corrosion inhibition: A review. *J. Mol. Liq.* **2021**, *322*, 114862. [CrossRef]
62. Shahmoradi, A.R.; Talebibahmanbigloo, N.; Nickhil, C.; Nisha, R.; Javidparvar, A.A.; Ghahremani, P.; Bahlakeh, G.; Ramezanzadeh, B. Molecular-MD/atomic-DFT theoretical and experimental studies on the quince seed extract corrosion inhibition performance on the acidic-solution attack of mild-steel. *J. Mol. Liq.* **2022**, *346*, 117921. [CrossRef]